Short communication

Catalytic hydrogen/oxygen reaction assisted the proton exchange membrane fuel cell (PEMFC) startup at subzero temperature

Shucheng Sun [a], Hongmei Yu [a,*], Junbo Hou [a,b], Zhigang Shao [a],
Baolian Yi [a], Pingwen Ming [c], Zhongjun Hou [c]

[a] *Fuel Cell R&D Center, Dalian Institute of Chemical Physics, Chinese Academy of Sciences, 457 Zhongshan Road, Dalian 116023, PR China*
[b] *Graduate School of the Chinese Academy of Sciences, Beijing 100039, PR China*
[c] *Dalian Sunrise Power Co., Ltd., 1# Huoju Road Qixianling, Dalian Hi-Tech Zone, Zhongshan Road, Dalian 116025, PR China*

Abstract

Fuel cells for automobile application need to operate in a wide temperature range including freezing temperature. However, the rapid startup of a proton exchange membrane fuel cell (PEMFC) at subfreezing temperature, e.g., $-20\,^{\circ}$C, is very difficult. A cold-start procedure was developed, which made hydrogen and oxygen react to heat the fuel cell considering that the FC flow channel was the characteristic of microchannel reactor. The effect of hydrogen and oxygen reaction on fuel cell performance at ambient temperature was also investigated. The electrochemical characterizations such as I–V plot and cyclic voltammetry (CV) were performed. The heat generated rate for either the single cell or the stack was calculated. The results showed that the heat generated rate was proportional to the gas flow rate when H_2 concentration and the active area were constant. The fuel cell temperature rose rapidly and steadily by controlling gas flow rate.
© 2007 Elsevier B.V. All rights reserved.

Keywords: PEMFC; Cold startup; Subzero temperature; Microchannel reactor; Hydrogen catalytic reaction

1. Introduction

Proton exchange membrane fuel cell (PEMFC) is widely considered as a promising energy conversion system for the future. However, water in PEMFCs might freeze at subzero temperature, which makes the cold-start capability and survivability a great challenge for automotive and outdoor applications. Now, fundamental mechanisms of the subzero startup dynamics are not fully understood, but it is recognized that product water forms ice or frost, accumulating in the cathode catalyst layer (CL), thereby reducing the oxygen reduction reaction and hindering the oxygen diffusion. When the cathode CL is plugged by the product ice, the PEMFC shuts down. Repetitive ice formation and melting in the CL may induce structural damage to the membrane electrode assembly (MEA).

Now, PEMFC storage and cold startup at subzero temperature have attracted increasing attention [1–8]. Although the cold-start capability of PEMFC is critically important, the relevant literature is very scarce. Since it is impossible for fuel cell to self-start from $-20\,^{\circ}$C, heating is necessary. Now, the cold-start methods were referred as follows [9]: resistance heat using DC from batteries, coolant heating, and hot air blowing. Since the mentioned methods might increase the volume and the weight of the system, the operation complexity and installation costs of the system will also increase.

Ahluwalia and Wang [10] used H_2 and O_2 mixture catalytic reaction to raise the fuel cell temperature, but they focused on the mixture out of explosive limits (4–74.2 vol% in O_2). Because the dimension of fuel cell flow channel (800 μm × 400 μm) is less than the quenching distance (1000 μm) [11] for H_2/O_2, which is in the dimension scale of microchannel reactor (MCR). It is well known that MCR possesses characteristics as high-heat transfer and high-specific surface area, thus the radicals are easily terminated on wall. As a result, the flame propagation can be inhibited in the MCR [12]. Veser [13] also reported that explosion limit depended on the reaction conditions such as temperature, pressure and reactor dimension. So the H_2/O_2 catalytic reaction can operate in a wide H_2 concentration range.

* Corresponding author. Tel.: +86 411 84379051; fax: +86 411 84379185.
  E-mail address: hmyu@dicp.ac.cn (H. Yu).

2. Experimental

2.1. The single cell and stack fabrication

The first single cell consisted of a MEA and two metal end-plates. The MEA was formed by hot pressing membrane with two gas diffusion layers (GDLs) at $140\,^\circ$C and 1 MPa for 1 min. The active area of MEA was $4\,cm^2$. Both endplates acted as the current collectors, which were machined with parallel flow channels. The endplates were silvered, and drilled in the middle. The thermal couple was placed in the hole of the cathode end-plate, and applied to measure the single cell temperature. The single cell was insulated by using polystyrene foam.

The second single cell consisted of a MEA and two metal current collectors. The active area of the MEA was $128\,cm^2$. The cell was insulated and the temperature of the cathode outlet was measured.

The fuel cell stack consisted of 10 cells with $245\,cm^2$ active area. At the rated power, each cell generated 110 W at 0.6 V. The temperature was measured at the current collector in the stack and the outlet of the stack. The stack was also insulated by using polystyrene foam. After removing water, the stack was put into a climate chamber. The stack was hold at $-20\,^\circ$C for 6 h and froze completely.

The flow field of the second single cell and stack were made of graphite. In general, the width of flow channel is 500–900 μm, its depth is 300–500 μm.

2.2. Relative humidity (RH) and polarization curve measurement

The values of the RH were obtained by using a hygrometer (Vaisala HMT360, Finland), thus we can know the degree of H_2 catalytic reaction. The hygrometer was placed at the outlet of the cathode side.

The cell was operated at $50\,^\circ$C, while H_2/O_2 humidification temperatures were set at $60\,^\circ$C and $65\,^\circ$C, the H_2/O_2 flow rates were controlled at $80\,ml\,min^{-1}$. The heating tape temperature was $5\,^\circ$C higher than the humidification temperatures to avoid water condensation. The single cell was operated at $1.2\,A\,cm^{-2}$ for 0.5 h, until the voltage became stable. Then, the polarization curve was recorded.

2.3. Cyclic voltammetry (CV) and H_2 concentration measurement of FC outlet

The CV measurement of the single cell was carried out to get the electrochemical surface area (ECSA) of Pt catalyst. For CV measurements, the humidified nitrogen and hydrogen was fed to the cathode and the anode, respectively. The cathode and the anode acted as a working and a counter electrode, respectively. The ECSA is related to the charge area under the H-desorption peak in the CV curve, the charge area of the H-desorption on the smooth Pt and the catalyst loading in the catalyst layer. The adsorption/desorption charge density for the hydrogen mono-layer on platinum is $210\,\mu C\,cm^{-2}$. The catalyst loading of the single cell is $0.4\,mg\,cm^{-2}$.

Table 1
Effect of H_2 concentration on fuel cell temperature and explosion probability

Flow, V_{H_2}/V_{total} (%)	$\Delta T/t$ ($^\circ$C min^{-1})	Outlet RH (%)	Explosion
4	0	68–87.1	No
10	0.1	65–86.7	No
20	1	–	No
30	2.1	–	No
40	3.1	90–94.2	No

The H_2 concentrations in the single cell and stack outlet were measured by gas chromatogram.

3. Results and discussion

3.1. Effect of hydrogen concentration on fuel cell temperature and the explosion probability

To investigate the effect of hydrogen concentration on heat generating rate and explosion possibility, the first single cell was used to carry out catalytic hydrogen reaction. The total gas flow rate was $100\,ml\,min^{-1}$ into the cathode. The initial temperature of fuel cell was $25\,^\circ$C. The hydrogen flow rate was in the range of $4–40\,ml\,min^{-1}$. Table 1 shows the temperature and the RH values of the fuel cell outlet increased with the hydrogen flow rate increase, when H_2 concentration is less than 40 vol%, the single cell did not explode. Since the fuel cell is actually a microchannel reactor, it is safe at normal explosion limit.

3.2. Effect of H_2 catalytic reaction on fuel cell performance

To investigate the performance change, we measured the single cell performance after the catalytic reaction at different hydrogen concentrations. Fig. 1 shows the three polarization curves. The "0" represents the single cell performance before the catalytic reaction, the "15%" and "40%" represent the polarization curves obtained after H_2 catalytic reaction at concentrations of 15% and 40% in the mixed gas, respectively. It can be seen that the hydrogen/oxygen catalytic reaction does not have negative impact on the fuel cell performance, when the H_2 concentra-
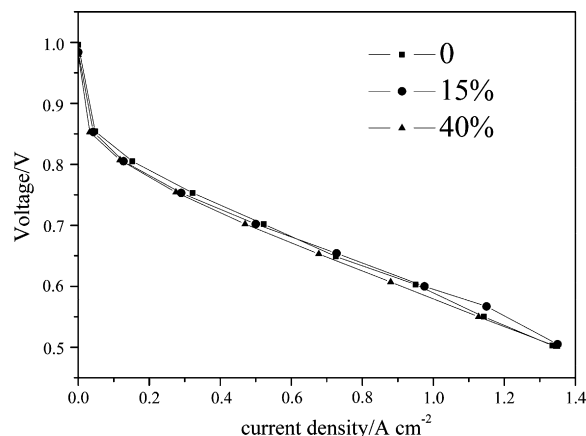

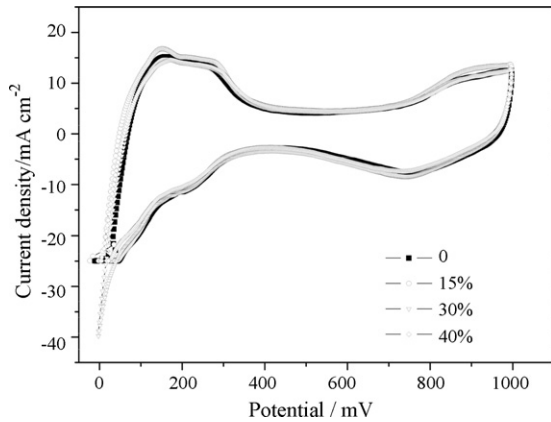Fig. 1. Polarization curves at different hydrogen concentrations of catalytic reactions.

Fig. 2. Cyclic voltammetry (CV) of catalytic reaction at different hydrogen concentrations.

tion is less than 40% volumetric (total gas flow rate is fixed at 100 ml min^{-1}).

The ECSA of platinum is one of the most important performance-determining factors in PEMFCs. Fig. 2 shows the CV curves after catalytic reaction at different hydrogen concentrations. The ECSA can be calculated with the following equation [14]:

$$\text{ECSA} \, (\text{m}^2\text{g}^{-1})$$
$$= \frac{\text{area charge } (\text{mC cm}^{-2})}{(10 \times 210 \, (\mu\text{C cm}^{-2})) \times \text{loading catalyst} \, (\text{mg cm}^{-2})}.$$

The charge density of the H$_2$ desorption peak of MEA are integrated and listed in Table 2. From Table 2, the values of the ECSA change between 46.68 m^2 g^{-1} and 55 m^2 g^{-1} for the single cell, without obvious decay.

3.3. Effect of the gas flow rate on the heat generating rate

To investigate the effect of gas flow rate on heat generating rate, we vary the hydrogen and oxygen flow rate into fuel cell and H$_2$ concentration is fixed to 30 vol%. Total gas flow rate varies from 100 ml min^{-1} to 1000 ml min^{-1}, which is fed into the cathode. Table 3 shows that the temperature and the RH of the fuel cell increase with the gas flow rate increase. The highest flow rate is about 20 times of the value when the current density is 1.0 A cm^{-2}, the H$_2$/O$_2$ flow rate is 350/700 ml min^{-1}. As summarized in Table 3, it is clear that the heat generating rate is proportion to the reactant flow rate. It indicates that the temperature of the fuel cell can be controlled by regulating the hydrogen/oxygen flow rate.

Table 2
Effects of catalytic reaction at different hydrogen concentrations on ECSA

H$_2$ concentration (%)	Charge density (mC cm^{-2})	ECSA (m^2 g^{-1})
0	41.96	49.95
15	46.24	55
30	39.20	46.68
40	43.09	51.3

Table 3
The heat generating rate of different gas flow rates

V_{H_2}/V_{O_2} (ml min^{-1})	$\Delta T/t$ (°C min^{-1})	Outlet RH (%)
30/70	0.9	84.2
60/140	1.97	86.2
90/210	4.9	84.2
210/490	6.32	90.4
300/700	8.79	94.3

3.4. Effect of the total gas flow rate on fuel cell performance

Effect of the gas flow rate on performance was investigated by measuring I–V curves after hydrogen catalytic reaction. The polarization curves are shown in Fig. 3. The hydrogen concentration is held at 30% in the experiments, and the total gas flow rate is increased gradually. The "0" represents the single cell polarization plot before the catalytic reaction, and the others represent the polarization curves after the catalytic reaction at different total gas flow rates. The I–V curves of the single cell show no change. During the catalytic reaction, the H$_2$ concentration of the single cell outlet was about 20%, which is in the explosion limit. However, no explosion occurred, which suggests that the chain reaction is terminated at FC outlet.

3.5. Effect of hydrogen catalytic reaction on heat generating rate of different active areas cell at subzero temperature

With the method mentioned above, the first single cell cold startup at −10 °C is studied. The flow rate of H$_2$/O$_2$ is 300/700 ml min^{-1}, respectively. As shown in Fig. 4, the single cell temperature increases rapidly to −9.4 °C in 30 s. Whereas heat generated is not sufficient to warm the fuel cell, and some generated water freezes and blocks the porous GDL, which results in the reactant "starvation", thus the fuel cell temperature does not increase.

Fig. 5 shows the startup process of the second single cell at −20 °C. Hydrogen concentration is fixed to 20%, and total gas flow rate gradually decreases. As shown in Fig. 5, the single cell temperature increases rapidly to 0 °C in 6 min. From
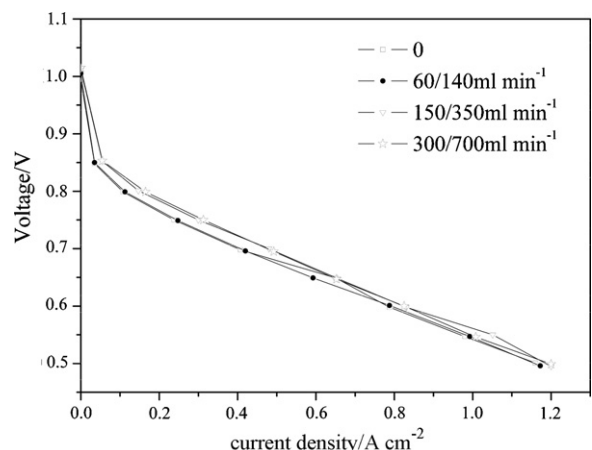

Fig. 3. Polarization curves of catalytic reaction at different gas flow rates.

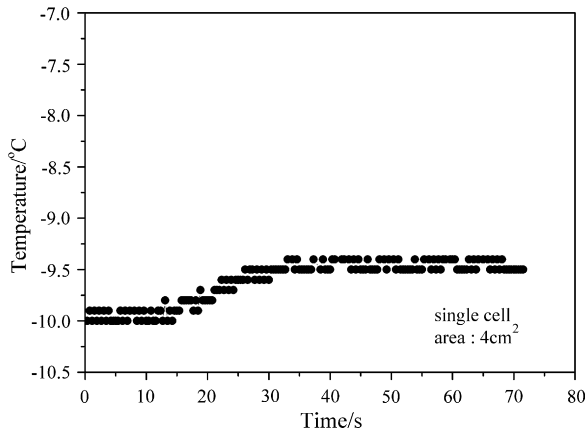Fig. 4. Temperature plot of catalytic hydrogen reaction at $-10\,°C$.

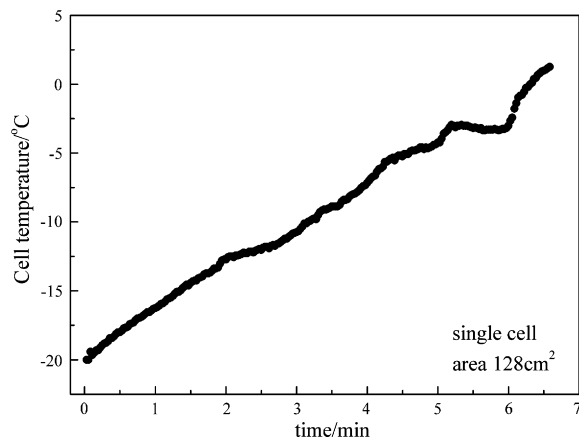
Fig. 5. Temperature plot of catalytic hydrogen reaction at $-20\,°C$.

Figs. 4 and 5, it can be seen that the bigger effective area of cell is, the faster heat generating rate is.

Figs. 6 and 7 show the process of the kW-class stack cold start. When the stack temperature approaches to $0\,°C$, the mixed gas stops. The stack is purged rapidly by N_2, and then the H_2/O_2 is fed to the anode and the cathode, respectively. The electronic load starts up. Fig. 6 presents the stack temperature during the catalytic hydrogen reaction and startup at $-20\,°C$. The inner
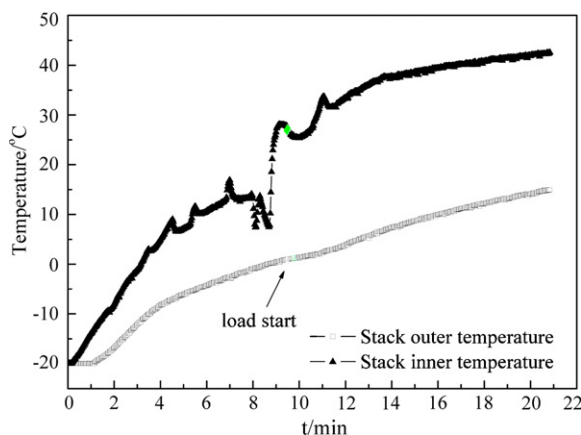

Fig. 6. Temperature plots of stack catalytic hydrogen reaction and startup at $-20\,°C$.

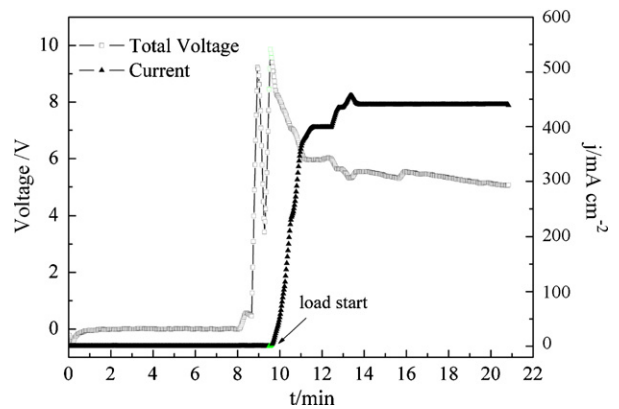Fig. 7. I–V plot of stack catalytic hydrogen reaction and startup at $-20\,°C$.

temperature represents the gas temperature, and the outer temperature stands for the stack temperature. Although the heat transfer is fast for the microchannel reactor, gas specific heat is smaller than the stack thermal capacity. So the stack temperature increase is hysteretic comparing with the gas increase. For example, when the gas temperature increased to $0\,°C$ in 3 min, the stack temperature was still at $-10\,°C$. The gas flow rate decreases gradually to prevent overheating. Fig. 7 shows the I–V curves of the catalytic hydrogen reaction and startup at $-20\,°C$. As it can be seen from Fig. 7, the average voltage is $0.6\,V$ at $400\,mA\,cm^{-2}$, finally the current density increased to $450\,mA\,cm^{-2}$. The stack performance is stable during the cold start. During the reaction, the H_2 concentration of the stack outlet was about 10%, but still no explosion occurred. This shows that the channel volume and surface property has strong impact on the chain propagation, and the explosion probability further decreased at $-20\,°C$. The characteristic of the FC microchannel easily makes the chain reaction terminate on the channel surface.

3.6. Heat balance of catalytic hydrogen reaction

The thermal capacity of fuel cell almost depends on the endplates and the bipolar plates, which is constant for the stack. So we roughly calculated the thermal capacity of the components of the stack at a constant power output. The heat generated rate is calculated, as follows

$$Q_g = Q_{stack} + Q_{gas}$$

where Q_g is the heat generated rate of the catalytic reaction, Q_{stack} is the heat up rate of stack and Q_{gas} is the heat up rate of gas. The stack temperature increased from $-20\,°C$ to $0\,°C$ in 9.5 min, and outlet gas temperature increased from $-20\,°C$ to $25\,°C$ in same time. Since the H_2/O_2 specific heat is quite small, the equation can be simplified, as follows

$$Q_g = Q_{stack}$$

The heat generated rate almost equals to the heat up rate of the stack, which decreases gradually with the increase of the stack temperature.

4. Conclusions

Rapid cold start of a PEMFC from subzero temperature is a challenge. Catalytic hydrogen reaction is an effective way to heat the fuel cell at open circuit. As the fuel cell flow channel is actually a microchannel reactor, the cold startup of the fuel cell stack by catalytic hydrogen reaction is safe when H_2 concentration is less than 20 vol%. Catalytic hydrogen reaction does not have negatively impact on fuel cell performance according to the CV and *I–V* results. Gas flow rate, gas concentration and active area are the key factors to increase the cell temperature and they are dependent on each other. When the active area and gas concentration are fixed, the gas flow rate is the control factor. The catalytic hydrogen reaction capacity of the fuel cell is very high. The startup is possible at $-20\,^\circ$C for the PEMFC stack by catalytic hydrogen reaction. Further work is necessary to accelerate the cold startup.

Acknowledgements

References

[1] E.A. Cho, J.-J. Ko, H.-Y. Ha, S.-A. Hong, K.-Y. Lee, T.-W. Lim, I.-H. Oh, J. Electrochem. Soc. 150 (2003) A1667.
[2] E.A. Cho, J.-J. Ko, H.-Y. Ha, S.-A. Hong, K.-Y. Lee, T.-W. Lim, I.-H. Oh, J. Electrochem. Soc. 151 (2004) A661.
[3] Y. Hishinuma, T. Chikahisa, F. Kagami, T. Ogawa, JSME Int. J. Ser. B 47 (2004) 235.
[4] M. Oszcipok, D. Riemann, U. Kronenwett, M. Zedda, J. Power Sources 145 (2005) 407.
[5] M. Oszcipok, M. Zedda, D. Riemann, D. Geckeler, J. Power Sources 154 (2006) 404.
[6] M. Oszcipok, M. Zedda, J. Hesselmann, M. Huppmann, M. Wodrich, M. Junghardt, C. Hebling, J. Power Sources 157 (2006) 666–673.
[7] Q. Yan, H. Toghiani, Y.-W. Lee, K. Liang, H. Causey, J. Power Sources 161 (2006) 492–502.
[8] J. Hou, H. Yu, S. Zhang, S. Sun, H. Wang, B. Yi, P. Ming, J. Power Sources 162 (2006) 513–520.
[9] A.A. Pesaran, G.H. Kim, J.D. Gonder, PEM Fuel Cell Freeze and Rapid Startup Invsetigation, National Renewable Energy Laboratory, 2005.
[10] R.K. Ahluwalia, X. Wang, DOE Workshop on Fuel Cell Operations at Sub-Freezing Temperatures, Argonne National Laboratory, Phoenix, AZ, February 1-2, 2005.
[11] B. Lweis, G. vonElbe, Combustion and Flames and Explosions of Gases, Academic Press, New York, 1987.
[12] I.M. Hsing, R. Srinivasan, M.P. Harold, K.F. Jensen, M.A. Schmidt, Chem. Eng. Sci. 55 (2000) 3–13.
[13] G. Vesr, J. Chem. Eng. Sci. 56 (2001) 1265–1273.
[14] T.R. Ralph, G.A. Hards, J.E. Keating, et al., J. Electrochem. Soc. 144 (1997) 3845.